OPTICS

Multidimensional entanglement transport through single-mode fiber

Jun Liu[1]*, Isaac Nape[2]*, Qainke Wang[1], Adam Vallés[2], Jian Wang[1]†, Andrew Forbes[1,2]

The global quantum network requires the distribution of entangled states over long distances, with substantial advances already demonstrated using polarization. While Hilbert spaces with higher dimensionality, e.g., spatial modes of light, allow higher information capacity per photon, such spatial mode entanglement transport requires custom multimode fiber and is limited by decoherence-induced mode coupling. Here, we circumvent this by transporting multidimensional entangled states down conventional single-mode fiber (SMF). By entangling the spin-orbit degrees of freedom of a biphoton pair, passing the polarization (spin) photon down the SMF while accessing multiple orbital angular momentum (orbital) subspaces with the other, we realize multidimensional entanglement transport. We show high-fidelity hybrid entanglement preservation down 250 m SMF across multiple 2 × 2 dimensions, confirmed by quantum state tomography, Bell violation measures, and a quantum eraser scheme. This work offers an alternative approach to spatial mode entanglement transport that facilitates deployment in legacy networks across conventional fiber.

INTRODUCTION

Entanglement is an intriguing aspect of quantum mechanics with well-known quantum paradoxes such as those of Einstein-Podolsky-Rosen (EPR) (*1*), Hardy (*2*), and Leggett (*3*). Yet, it is also a valuable resource to be harnessed: Entangled particles shared with different distant observers can be used in quantum cryptography to set an unconditional secure key (*4*, *5*), in quantum teleportation to transfer quantum information (*6*–*10*), in super-dense coding (*11*, *12*), in ghost imaging (*13*, *14*) and are also an important part of quantum computation (*15*–*17*).

In the past few decades, quantum entanglement has been extensively explored for a variety of quantum information protocols. Standard quantum communication protocols exploit polarization (or "spin" angular momentum) encoding with single photon and multipartite states. Up to now, entanglement transport has been verified over distances up to 1200 km via free space (satellite-based distribution) (*18*) and over 100 km through fiber using polarization-entangled photons (*19*, *20*). Exploiting high-dimensional entangled systems presents many opportunities, for example, a larger alphabet for higher photon information capacity and better robustness to background noise and hacking attacks (*21*, *22*), increasing the storage capacity in quantum memories as well (*23*, *24*). High-dimensional systems have been studied by correlations in various degrees of freedom, including position time (*25*), energy time (*26*, *27*), time bin (*28*–*30*), time frequency (*31*), and frequency (*32*). More recently, the orbital angular momentum (OAM) of light, related to the photon's transverse mode spatial structure, has been recognized as a promising resource (*33*–*36*).

Despite these advances, quantum communication with spatial modes is still in its infancy, with reported entanglement transport in multimode fiber limited to less than 1 m (*37*, *38*) and to kilometer ranges using single-photon states (no entanglement) in specially designed custom multimode fiber (*39*), still orders of magnitude less than that with polarization, and lacking the ability to integrate into existing networks, a crucial element of any future quantum network (*40*–*42*). Moreover, the mooted benefits of high-dimensional states against noise have yet to be realized in the laboratory, while a measured channel capacity has been found to be twice higher by multiplexing two-dimensional subspaces rather than transmitting the full four high-dimensional states (*39*). This motivates us to seek alternative, immediately deployable solutions that are neither two-dimensional nor high-dimensional but rather "multidimensional."

Here, we demonstrate the transport of multidimensional entangled states down conventional single-mode fiber (SMF) by exploiting hybrid entangled states. We combine polarization qubits with high-dimensional spatial modes by entangling the spin-orbit (SO) degrees of freedom of a biphoton pair, passing the polarization (spin) photon down the SMF while accessing multidimensional OAM subspaces with the other photon in free space. We show high-fidelity hybrid entanglement preservation down 250 m of SMF across 2 two-dimensional subspaces (2 × 2 dimensions) in what we refer to as multidimensional entanglement. We quantify our one-sided channel by means of quantum state tomography, Bell inequality, and quantum eraser experiments. This work suggests an alternative approach to spatial mode entanglement transport in fiber, with the telling advantage of deployment over legacy optical networks with conventional SMF.

RESULTS

Concept and principle

The concept and principle of multidimensional spin-orbit entanglement transport through SMF are illustrated in Fig. 1. Light beams carrying OAM are characterized by a helical phase front of $\exp(i\ell\theta)$ (*43*), where θ is the azimuthal angle and $\ell \in [-\infty, +\infty]$ is the topological charge. This implies that OAM modes, in principle, form a complete basis in an infinitely large Hilbert space. However, the control of such high-dimensional states is complex, and their transport requires custom channels, e.g., specially designed custom multimode fiber. On the contrary, polarization is limited to just a two-level system but is easily transported down SMF. Here, we compromise between the two-level spin entanglement and the high-dimensional OAM entanglement to transport multidimensional spin-orbit hybrid

[1]Wuhan National Laboratory for Optoelectronics and School of Optical and Electronic Information, Huazhong University of Science and Technology, Wuhan 430074, Hubei, China. [2]School of Physics, University of the Witwatersrand, Private Bag 3, Wits 2050, South Africa.
*These authors contributed equally to this work
†Corresponding author. Email: jwang@hust.edu.cn

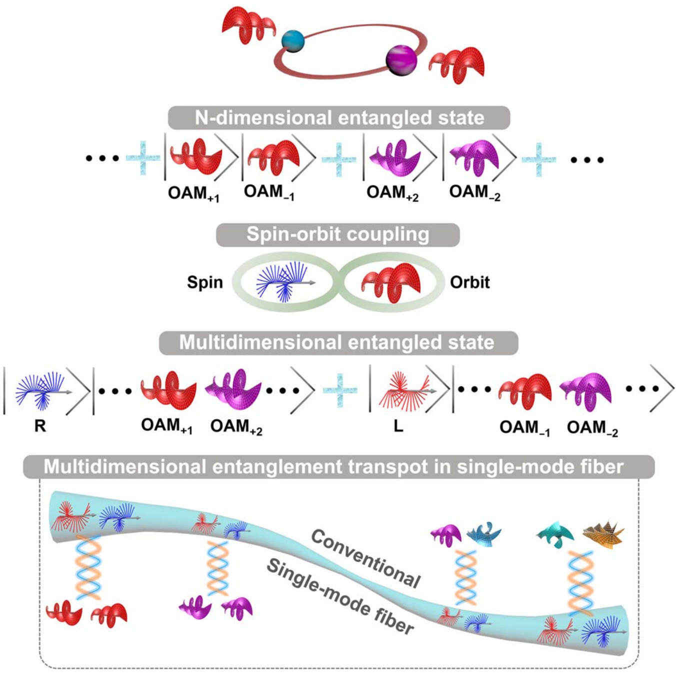

Fig. 1. Multidimensional entanglement transport through single-mode fiber. An initially high-dimensional state is converted by spin-orbit coupling into multiple two-dimensional hybrid entangled states. The polarization (spin) photon has a fundamental spatial mode (Gaussian), facilitating transport down an SMF. By hybrid entanglement, the infinite space of OAM is accessed by two-dimensional subspaces at a time.

entanglement. A consequence is that the entire high-dimensional OAM Hilbert space can be accessed but two dimensions at a time. We will demonstrate that, in doing so, we are able to transport multidimensional entanglement down conventional fiber.

To see how this works, consider the generation of OAM-entangled pairs of photons by spontaneous parametric down-conversion (SPDC). The biphoton state produced from the type I SPDC process can be expressed in the OAM basis as

$$|\psi\rangle_{AB} = \sum_{\ell} c_\ell \,|H\rangle_A\, |H\rangle_B\, |\ell\rangle_A\, |-\ell\rangle_B \tag{1}$$

where $|c_\ell|^2$ is the probability of finding photons A and B in the eigenstates $|\pm\ell\rangle$, respectively, and $|H\rangle$ is the horizontal polarization. Subsequently, one of the photons (e.g., photon A), from the N-dimensional OAM-entangled photon pair, is passed through a spin-orbit coupling (SOC) optics for OAM to spin conversion, resulting in a hybrid multidimensional polarization (spin) and OAM-entangled state

$$|\Psi^\ell\rangle_{AB} = \frac{1}{\sqrt{2}}(|R\rangle_A\,|\ell_1\rangle_B + |L\rangle_A\,|\ell_2\rangle_B) \tag{2}$$

Here, $|R\rangle$ and $|L\rangle$ are the right and left circular polarization (spin) eigenstates on the qubit space $\mathcal{H}_{A,\mathrm{spin}}$ of photon A, and $|\ell_1\rangle$ and $|\ell_2\rangle$ denote the OAM eigenstates on the OAM subspace $\mathcal{H}_{B,\mathrm{orbit}}$ of photon B. The state in Eq. 2 represents a maximally entangled Bell state where the polarization degree of freedom of photon A is entangled with the OAM of photon B. Each prepared photon pair can be mapped onto a density operator $\rho_\ell = |\Psi^\ell\rangle\langle\Psi^\ell|$ with $|\Psi^\ell\rangle \in \mathcal{H}_{A,\mathrm{spin}} \otimes \mathcal{H}_{B,\mathrm{orbit}}$ by actively switching between OAM modes sequentially in time: The larger Hilbert space is spanned by multiple two-dimensional subspaces, i.e., multidimensional states in the quantum channel. For simplicity, we will consider subspaces of $|\pm\ell\rangle$ but stress that any OAM subspace is possible, only limited by the SOC device characteristics. We can represent the density matrix of this system as

$$\rho_{AB} = \sum_{\ell=1}^{\infty} \gamma_\ell \rho_\ell \tag{3}$$

where γ_ℓ represents the probability of post-selecting the hybrid state ρ_ℓ. The density matrix pertaining to system related to photon B is

$$\rho_B = \mathrm{Tr}_A(\rho_{AB}) = \sum_{\ell=0}^{\infty} \frac{\gamma_\ell}{2}(|\ell\rangle_B\langle\ell|_B + |-\ell\rangle_B\langle-\ell|_B) \tag{4}$$

where $\mathrm{Tr}_A(\bullet)$ is the partial trace over photon A. While photon B is in a superposition of spatial modes (but a single spin state), photon A is in a superposition of spin states but only a single fundamental spatial mode (Gaussian), i.e., $|\psi\rangle_A \propto (|L\rangle + |R\rangle)|0\rangle$ and $|\psi\rangle_B \propto |H\rangle(|\ell\rangle + |-\ell\rangle)$. As a consequence, photon A can readily be transported down SMF while still maintaining the spatial mode entanglement with photon B. We stress that we use the term "multidimensional" as a proxy for multi-OAM states due to the variability of OAM modes in the reduced state of photon B: Any one of these infinite possibilities can be accessed by suitable SOC optics, offering distinct advantages over only 1 two-dimensional subspace as is the case with polarization.

Implementation

We prepare the state in Eq. 2 via postselection from the high-dimensional SPDC state. In this paper, the SOC optics is based on q plates (44). The q plate couples the spin and OAM degrees of freedom following

$$|R\rangle|\ell\rangle \xrightarrow{q-\text{plate}} |L\rangle|\ell-2q\rangle, \quad |L\rangle|\ell\rangle \xrightarrow{q-\text{plate}} |R\rangle|\ell+2q\rangle \tag{5}$$

where q is the topological charge of the q plate. Accordingly, the circular polarization eigenstates are inverted, and an OAM variation of $\pm 2q$ is imparted on the photon depending on the handedness of the input circular polarization (spin) state. Transmission of photon A through the SMF together with a detection acts as a postselection, resulting in the desired hybrid state (see the Supplementary Materials). Hence, considering N different OAM states $\pm\ell_n$ and N different q plates with different topological charge q_n (such as $\ell_n \pm 2q_n = 0$) would allow us to access $2 \times N$ dimensions using a single SMF.

The experimental setup for multidimensional spin-orbit entanglement transport through SMF is shown in Fig. 2A. A continuous-wave pump laser (Cobolt MLD diode laser, λ = 405 nm) was spatially filtered by a pinhole with a diameter of 100 μm to deliver 118 mW of average power in a Gaussian beam at the nonlinear crystal [a temperature-controlled 10-mm-long periodically poled potassium titanyl phosphate (PPKTP) crystal], generating two lower-frequency photons by means of a degenerate type I SPDC process. By virtue of this, the signal and idler photons had the same wavelength (λ = 810 nm) and polarization (horizontal). The residual pump beam was filtered out by a band-pass filter with a center wavelength of 810 nm and a bandwidth of 10 nm. The two correlated photons, signal and idler, were spatially separated by a 50:50 beam splitter (BS), with the signal photon

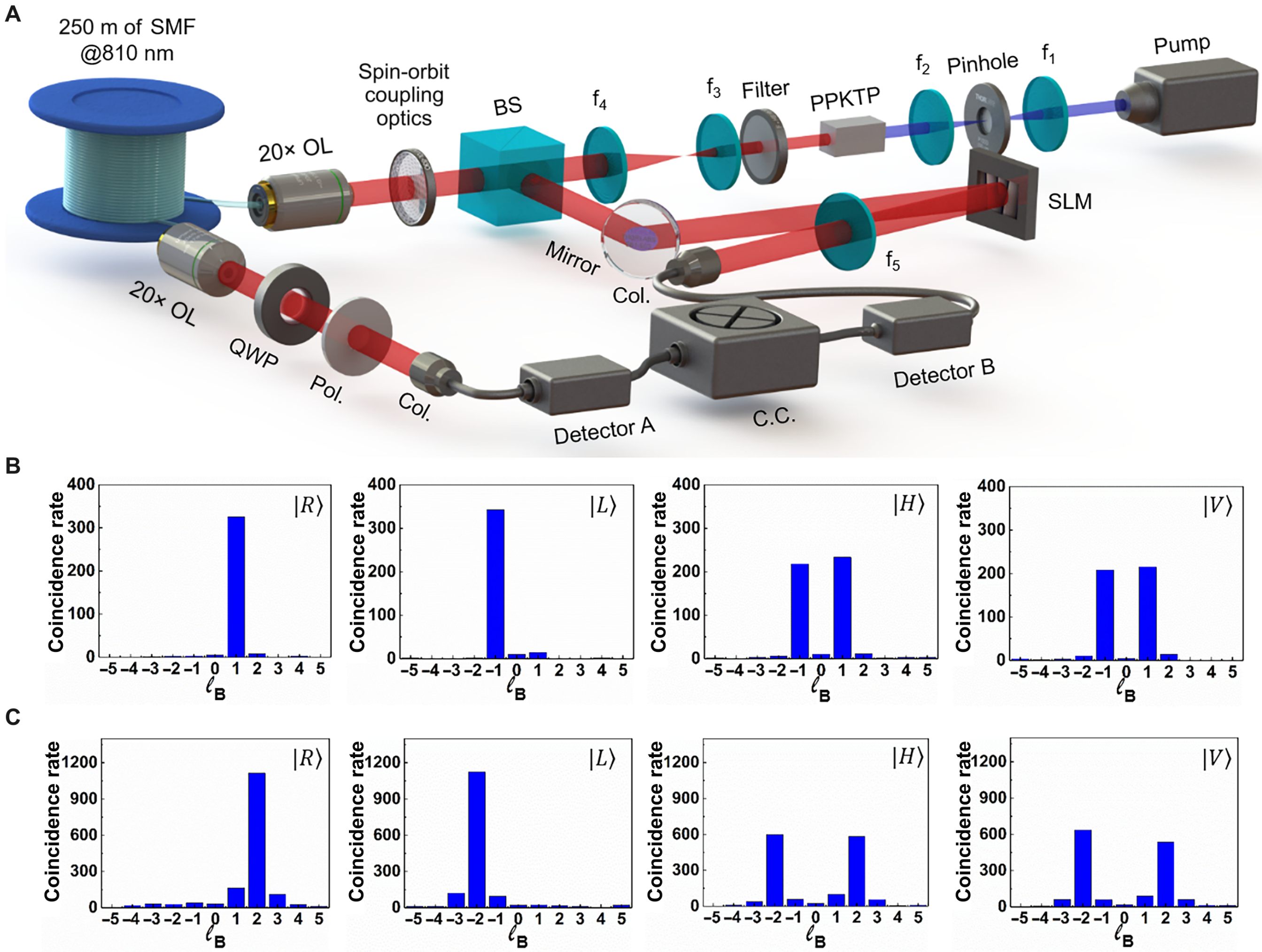

Fig. 2. Experimental setup and OAM transport. (**A**) Experimental setup. Pump, λ = 405 nm (Cobolt, MLD laser diode); f, Fourier lenses of focal length $f_{1;2;3;4;5}$ = 100, 100, 200, 750, and 1000 mm, respectively; PPKTP, periodically poled potassium titanyl phosphate (nonlinear crystal); Filter, band-pass filter; BS, 50:50 beam splitter; QWP, quarter–wave plate; Pol., polarizer; SLM, spatial light modulator; Col., collimator, f = 4.51 mm; CC, coincidence counter. (**B**) Measured coincidence count rate for the mode spectrum of the ℓ = ±1 subspace and (**C**) the ℓ = ±2 subspace after transmitting through 250 m of SMF. All coincidence rates are given as coincidences per second.

A interacting with the SOC optics, e.g., q plate, for orbit-to-spin conversion. Subsequently, photon A was coupled into the 250-m SMF by a 20× objective lens to transmit through the fiber and coupled out by another 20× objective lens. The idler photon B was imaged to the spatial light modulator (SLM) with lenses f_3 and f_4. After that, photon B was imaged again by f_5 and a collimator, being coupled into an SMF, and hence spatial filtered as well, for detection.

The projective measurements were done by the quarter–wave plate (QWP) along with a polarizer for photon A and SLM along with an SMF for photon B. Photon A, encoded with polarization eigenstates, was transmitted through the SMF, while photon B, encoded with multidimensional OAM eigenstates, was transported through free space. Last, both photons were detected by the single-photon detectors, with the output pulses synchronized with a coincidence counter.

Hybrid entanglement transport

We first evaluate the SMF quantum channel by measuring the OAM mode spectrum after transmitting through 250 m of SMF. Figure 2 (B and C, respectively) shows the mode spectrum of the ℓ = ±1 and ℓ = ±2 subspaces. We project photon A onto right circular polarization (R), left circular polarization (L), horizontal polarization (H), and vertical polarization (V) by adjusting the QWP and polarizer at the output of the fiber while measuring the OAM of photon B holographically with an SLM and SMF. The results are in very good agreement with a channel that is impervious to OAM. When the orthogonal polarization states are selected on photon A ($|L\rangle$ and $|R\rangle$), an OAM state of high purity is measured for photon B, approximately 93% for ℓ = ±1 and approximately 87% for ℓ = ±2. The slightly lower value for the ℓ = ±2 subspace is due to concatenation of two SOC optics for the hybrid entanglement step (see the Supplementary Materials and Methods).

To confirm the state and the entanglement conservation, we perform a full quantum state tomography on the hybrid state to reconstruct the density matrix. Figure 3 shows the state tomography measurements and resulting density matrices for both the ℓ = ±1 and ℓ = ±2 subspaces after 250 m of SMF, with the free space ℓ = ±1 shown as a point of comparison (see the Supplementary Materials for more results in free space and in 2 m of SMF). The fidelity against a maximally entangled state is calculated to be 95% for the $\ell = \pm 1$ and 92% for the $\ell = \pm 2$ subspaces. This confirms that the fiber largely maintains the fidelity of each state. Using concurrence (C) as our measure of entanglement (see Methods), we find $C = 0.91$ for free space, down slightly to $C = 0.9$ for $\ell = \pm 1$ and $C = 0.88$ for $\ell = \pm 2$.

The state tomography results depicted for each of the subspaces have different average coincidence count rates due to several small imperfections during the experimental realization: different collection efficiency depending on the detected spatial mode, temperature fluctuations in the nonlinear crystal oven causing a slight reduction in the SPDC efficiency, and some error in the rotation of the wave plates may have caused differences in the state tomography outcome depending on the projections. Nonetheless, the fidelity of the free-space density matrix is still higher owing to the minimal cross-talk between the orthogonal modes (across the diagonal).

To carry out a nonlocality test in the hybrid regime, we define the two sets of dichotomic observables for A and B: the bases a and $\tilde{a}$ of Alice correspond to the linear polarization states $\{|H\rangle, |V\rangle\}$ and $\{|A\rangle, |D\rangle\}$, respectively, while the bases b and $\tilde{b}$ of Bob correspond to the OAM states $\{\cos(\frac{\pi}{8})|\ell\rangle - \sin(\frac{\pi}{8})|-\ell\rangle, -\sin(\frac{\pi}{8})|\ell\rangle + \cos(\frac{\pi}{8})|-\ell\rangle\}$ and $\{\cos(\frac{\pi}{8})|\ell\rangle + \sin(\frac{\pi}{8})|-\ell\rangle, \sin(\frac{\pi}{8})|\ell\rangle - \cos(\frac{\pi}{8})|-\ell\rangle\}$. From the data shown in Fig. 4, we calculate the Clauser-Horne-Shimony-Holt (CHSH) Bell parameters in free space and through SMF (see Methods). We find CHSH Bell parameters of $S = 2.77 \pm 0.06$ and $S = 2.47 \pm 0.09$ for the $\ell = \pm 1$ subspace in free space and in 250 m of SMF, respectively, reducing to $S = 2.51 \pm 0.04$ and $S = 2.25 \pm 0.19$ for the $\ell = \pm 2$ subspace. In all cases, we violate the Bell-like inequality.

A hybrid quantum eraser

Next, we use the same experimental setup to demonstrate a hybrid quantum eraser across 250 m of SMF. We treat OAM as our "path" and the polarization as the "which path" marker to realize a quantum eraser with our hybrid entangled photons. We first distinguish the OAM (path) information in the system by marking the OAM eigenstates of photon B with linear polarizations of photon A. In this experiment, we achieve this by placing a QWP before a polarizer, transforming Eq. 2 to

$$|\tilde{\Psi}^{\ell}\rangle_{AB} = \frac{1}{\sqrt{2}}(|H\rangle_A|\ell_1\rangle_B + |V\rangle_A|\ell_2\rangle_B) \tag{6}$$

By selecting either polarization states, $|H\rangle$ or $|V\rangle$, the distribution of photon B collapses on one of the OAM eigenstates, $\ell_{1,2}$, having a uniform azimuthal distribution and fringe visibility of $V \equiv \frac{(\max-\min)}{(\max+\min)} = 0$, reminiscent of the smeared pattern that is observed from distinguishable (noninterfering) paths in the traditional quantum eraser (*45*). The OAM information can be erased by projecting photon A onto the complimentary basis of the OAM markers, i.e., $|\pm\rangle = \frac{1}{\sqrt{2}}(|H\rangle \pm |V\rangle)$, causing the previously distinguished OAM (paths) to interfere, thus creating azimuthal fringes that can be detected with an azimuthal pattern sensitive scanner. The fringes appear with a visibility of $V = 1$, indicative of OAM information reduction (*46*). The appearance in azimuthal fringes of photon B is indicative of OAM information being erased from photon B. It is noteworthy to point out that, here, the QWP acts as the path marker, while the polarizer acts as the eraser. Notably,

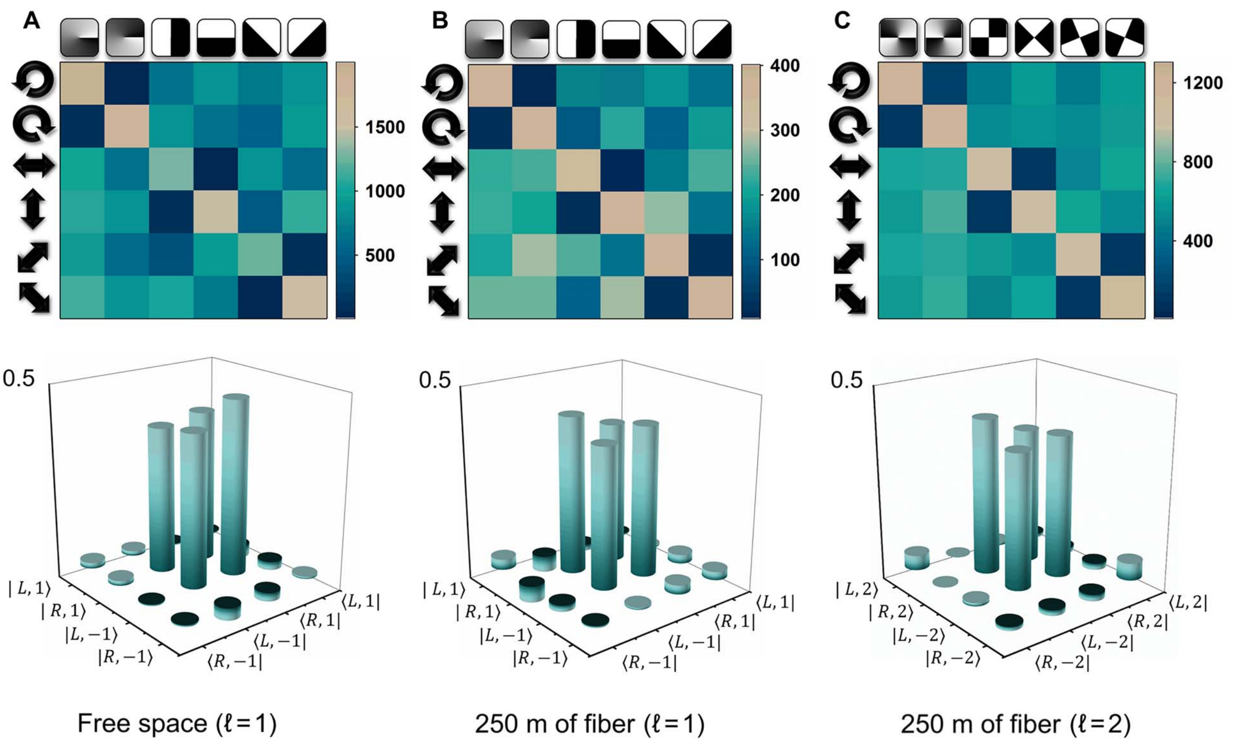

Fig. 3. Quantum state tomography of hybrid multidimensional states. (**A**) $\ell = \pm 1$ in free space for system verification with (**B**) $\ell = \pm 1$ and (**C**) $\ell = \pm 2$ subspaces after transmitting the hybrid state through a one-sided 250-m SMF channel. The top panels show the raw tomography data for the 6 × 6 projections, the rows representing polarization measurements on photon A and the columns representing holographic measurements on photon B. The bottom panels show the outcome of the tomography, a density matrix for each subspace.

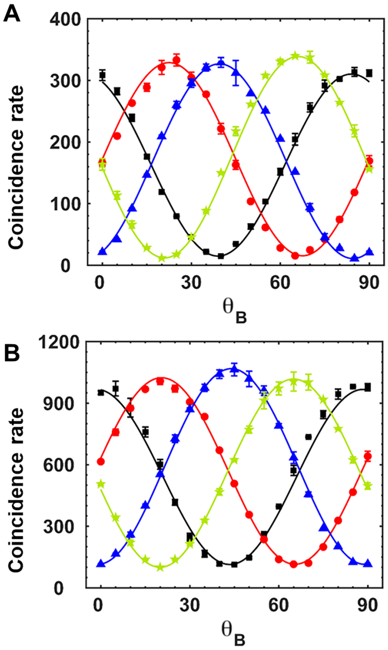

Fig. 4. Hybrid state Bell violations. Measured correlations between photon A (polarization) and photon B (OAM) in (**A**) the ℓ = ±1 subspace after 250 m of SMF and (**B**) the ℓ = ±2 subspace after 250 m of SMF. Photon A is projected onto the states $\theta_A = \left\{\frac{3\pi}{2}, \pi, \frac{\pi}{2}, 0\right\}$, corresponding to A, V, D, and H polarization states and known to maximally violate the Bell inequality, while the superposition hologram is rotated in arm B through an angle θ_B. All coincidence rates are given as coincidences per second.

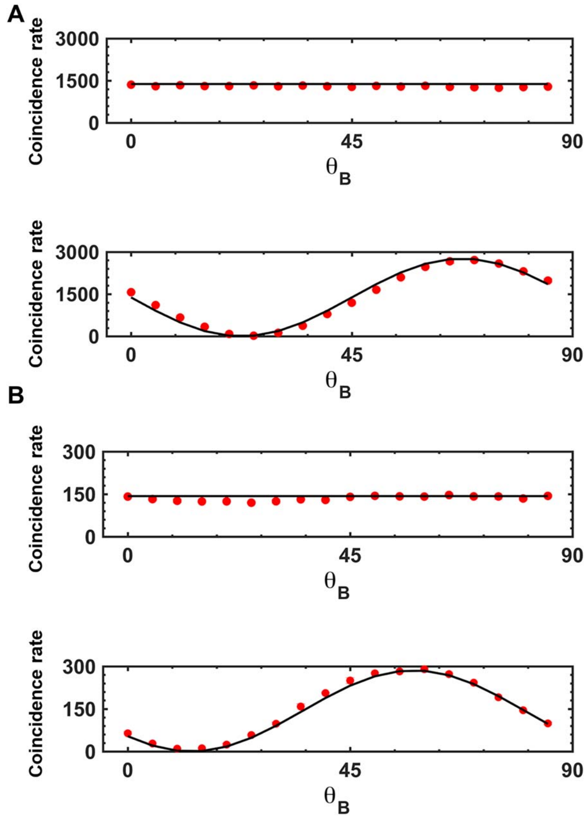

Fig. 5. A hybrid quantum eraser through fiber. Experimental coincidence count rates for distinguishing and erasing the OAM, in the ℓ = ±1 subspace, of photon B upon transmitting photon A through (**A**) free space and through (**B**) 250-m SMF. OAM (path) information is introduced into the system with a QWP, and a polarizer selecting one of the markers. Here, we select the state $|H\rangle$ and, as seen, the spatial distribution of photon B is uniform with minimal visibility. In the complimentary case, the path markers collapse onto a superposition $|+\rangle$ or equivalently $|D\rangle$, with the polarizer and all the path information removed, manifesting as prominent visible azimuthal fringes. All coincidence rates are given as coincidences per second.

complementarity between path information and fringe visibility (V) is essential to the quantum eraser. By defining the two distinct paths using the OAM degree of freedom, we find that it is possible to distinguish ($V = 0.05 \pm 0.01$) and erase ($V = 0.98 \pm 0.002$) the OAM path information of a photon through the polarization control of its entangled twin in free space, as shown in Fig. 5. With only marginal loss of visibility after transmitting through 250 m of SMF, the entanglement is conserved with the ability to distinguish ($V = 0.11 \pm 0.01$) and erase ($V = 0.93 \pm 0.01$) the OAM path information.

Although the eraser procedure was performed on the ℓ = ±1 subspace, it can be extended to higher subspaces: Depending on the SOC device that is used for photon A, the SLM holograms implemented for scanning the azimuthal fringes of photon B can be adapted to the relevant subspace.

DISCUSSION AND CONCLUSION

In our work, any two-dimensional subspace of the high-dimensional space is accessible by simply changing the SOC optics. In our experiment, we used two sets of the SOC optics, each for selecting ℓ = ±1 to reach ℓ = ±2; this introduced additional distortions that were reflected in the lower performance as compared to ℓ = ±1. Nevertheless, even with this arrangement, the entanglement was still preserved over an extended distance of 250 m, which we have demonstrated through quantum state tomography, Bell inequality violations, and a novel quantum eraser experiment. Moreover, the demonstration of 2 two-dimensional subspaces is double what would be possible with only polarization entanglement. While we used OAM states of $\{|\ell\rangle, |-\ell\rangle\}$, it is possible to select any two orthogonal OAM states from the N-dimensional space to establish the OAM basis, i.e., $\{|\ell_1\rangle, |\ell_2\rangle\}\ \forall\ \ell_1 \neq \ell_2$. In addition, one can also choose any orthogonal polarization states, for example, $\{|R\rangle, |L\rangle\}$, $\{|H\rangle, |V\rangle\}$, or $\{|A\rangle, |D\rangle\}$. This can be done by specially designed SOC optics and has already been demonstrated classically (*47*). In this way, our work may be extended by judiciously selecting states for reducing coupling with the environment and therefore preserve the entanglement of the system over even longer distances.

Excitingly, our work opens a new path toward multiplexed quantum key distribution (QKD) down conventional SMF. Multiplexed QKD has been demonstrated with OAM modes down custom optical fiber and shown to double the key rate of transmitting a four-dimensional state (*39*). In our approach, each spatial mode, e.g., the OAM modes, would correspond to an independent channel, as long as all counterparts are postselected with different ℓ, forming an interesting rerouting quantum optical hub. In addition to deployment over conventional fiber, this multiplexing advance requires only the use of already existing technology in the form of OAM mode sorters (*48*).

Our scheme offers an alternative to high-dimensional entanglement transport over long distance, the latter limited by both fundamental and practical issues. These include the need for multiple photons to teleport high dimensions (*49*), the excessively long measurement times to reconstruct such states (*50*), and the difficulty in experimental execution of high-dimensional spatial mode teleportation (*51*). The mooted benefits of high-dimensional states are likewise yet to be realized experimentally: Robustness to noise has not been shown for spatial mode entanglement, while existing models consider only white noise and not the more troublesome modal coupling noise terms. Further, the benefit is derived in part from the existence of K-dimensional entanglement in the initial D-dimensional state but without any recipe for finding or specifying what K might be. Because of these issues, laboratory QKD (in specialty fiber) has revealed that it is far better to use the higher dimensions for multiplexing than it is to encode information directly in them. Our approach is a compromise that reaps the benefits of multiple states while allowing immediate deployment across legacy networks. No other spatial mode solution allows this.

In conclusion, we have outlined a new approach to transporting entanglement through fiber in a manner that allows deployment over a conventional network of SMF. The result is based on hybrid entangled states, allowing access to multiple dimensions: an infinite number of two-dimensional subspaces. Together, these subspaces span the entire high-dimensional Hilbert space that would be available by spatial mode entanglement. Our experimental demonstration over 250 m of SMF and at double the dimensions available to polarization shows that this scheme is a viable approach to circumvent the technological hurdles of deploying spatial mode entanglement.

METHODS

Fidelity

We calculate the fidelity of our states from (*52*)

$$F = \mathrm{Tr}(\sqrt{\sqrt{\rho_T}\rho_P\sqrt{\rho_T}})^2 \tag{7}$$

where ρ_T is the density matrix representing a target state and ρ_P is the predicted (or reconstructed) density matrix taking values ranging from 0 to 1 for $\rho_T \neq \rho_P$ and $\rho_T = \rho_P$, respectively. For a target state that is pure, such as the given in Eq. 2, i.e., $\rho_T = |\Psi^\ell\rangle\langle\Psi^\ell|$, the fidelity can be also expressed as

$$F = \mathrm{Tr}[\rho_T\rho_P] = \langle\Psi^\ell|\rho_P|\Psi^\ell\rangle \tag{8}$$

Concurrence

We use the concurrence as our measure of entanglement, calculated from

$$C_\Theta(\rho) = \max\{0, \lambda_1 - \sum_{i=2}\lambda_i\} \tag{9}$$

where ρ is the density matrix of the system being studied (mixed or pure), λ are the eigenvalues of the operator $R = \sqrt{\rho}\sqrt{\tilde{\rho}}$ in descending order with $\tilde{\rho} = \Theta\rho^*\Theta$, and * denotes a complex conjugation. The operator Θ represents any arbitrary anti-unitary operator satisfying $\langle\psi|\Theta|\phi\rangle = \langle\phi|\Theta^{-1}|\psi\rangle$ for any state $|\phi\rangle$ and $|\psi\rangle$, if $\Theta^{-1} = \Theta^\dagger$.

Density matrix on a hybrid state space

The density matrix of a single photon in a two-dimensional state space ($\mathcal{H}_2$) can be represented as a linear combination of the Pauli matrices (*53*)

$$\rho = \frac{1}{2}(\mathbb{I}_0 + \sum_{3}^{k=1} b_k\sigma_k) \tag{10}$$

where $\mathbb{I}_0$ is the two-dimensional identity operator and σ_k are the traceless Pauli operators with complex coefficients b_k. In this work, we consider the density matrix of a hybrid entangled state similar to Eq. 2. It can be expressed as

$$\rho = \frac{1}{2}(\mathbb{I}_A\otimes\mathbb{I}_B + \sum_{3}^{m,n=1} b_{mn}\sigma_{Am}\otimes\sigma_{Bn}) \tag{11}$$

where $\mathbb{I}_{AB}$ is the two photon identity matrix and σ_{Am} and σ_{Bn} are the Pauli matrices that span the two-dimensional hybrid space for polarization and OAM, respectively.

Quantum state tomography

We reconstruct each hybrid state, ρ_ℓ, via quantum state tomography. This entails performing a series of local projections $M_{ij} = P_A^i\otimes P_B^j$, where $P_{A,B}^{i,j}$ are projections on photon A and photon B, respectively, and using the resulting measurement outcomes to reconstruct the state (*54*). The detection probabilities on a system with a corresponding density matrix (ρ) are

$$p_{ij} = Tr[M_{ij}\rho M_{ij}^\dagger] \tag{12}$$

The overall projections constitute an over-complete set of measurements on the two photon subspace. In the experiment, photon A was projected onto the spin basis states $|R\rangle$ and $|L\rangle$, along with their equally weighted superpositions of linear antidiagonal, diagonal, horizontal, and vertical polarization states, i.e., $|A\rangle$, $|D\rangle$, $|H\rangle$, and $|V\rangle$, respectively. Similarly, photon B was locally projected onto the eigenstates $|\pm\ell\rangle$ along with superpositions

$$|\theta\rangle = \frac{1}{\sqrt{2}}(|\ell\rangle + e^{i\theta}|-\ell\rangle) \tag{13}$$

for relative phase $\theta = \frac{3\pi}{2}, \pi, \frac{\pi}{2}, 0$.

CHSH Bell violation

To further characterize the nonlocal correlations in each hybrid subspace, a violation of the CHSH Bell inequality (*55*) with the two-photon system is used. First, we project photon B onto the states, $\theta_A = \{\frac{3\pi}{2}, \pi, \frac{\pi}{2}, 0\}$, corresponding to A, V, D, and H polarization states, while we measure the photon coincidence rate as a function of θ_B (relative phase between $|\ell\rangle$ and $|-\ell\rangle$ in arm B). The variation of the number of coincidences with the angle θ_B is in agreement with expected nonclassical correlations. We define the CHSH Bell parameter S as (*56*)

$$S = |E(\theta_A, \theta_B) - E(\theta_A, \theta'_B) + E(\theta'_A, \theta_B) + E(\theta'_A, \theta'_B)| \tag{14}$$

with $E(\theta_A, \theta_B)$ calculated from coincidence events

$$
\begin{aligned}
E(\theta_A,\theta_B) &= \frac{\xi(\theta_A,\theta_B)-\xi'(\theta_A,\theta_B)}{\xi(\theta_A,\theta_B)+\xi'(\theta_A,\theta_B)},\\
\xi(\theta_A,\theta_B) &= C(\theta_A,\theta_B)+C\left(\theta_A+\frac{\pi}{2},\theta_B+\frac{\pi}{2}\right),\\
\xi'(\theta_A,\theta_B) &= C\left(\theta_A+\frac{\pi}{2},\theta_B\right)+C\left(\theta_A,\theta_B+\frac{\pi}{2}\right).
\end{aligned}
\tag{15}
$$

Here, $C(\theta_A, \theta_B)$ represents measured coincidence counts. The Bell parameter can be characterized as $S \le 2$ for separable states and $2 < S \le 2\sqrt{2}$ for maximally entangled states.

SUPPLEMENTARY MATERIALS

Supplementary material for this article is available at http://advances.sciencemag.org/cgi/content/full/6/4/eaay0837/DC1

Additional results of mode spectrum, tomography measurements and reconstructed density matrices for subspace in free space and subspace after transmitting through 2 m of SMF

Additional results of correlations between photon A (polarization) and B (OAM)

Additional results of fidelity and concurrence from quantum tomography

Fig. S1. Additional results of measured mode spectrum.

Fig. S2. Additional results of tomography measurements and reconstructed density matrices.

Fig. S3. Additional results of Bell violations and quantum eraser measurements.

Table S1. Fidelity and concurrence values in free space, through 2 m of SMF and 250 m of SMF for ℓ = ±1 and ℓ = ±2 subspaces.

REFERENCES AND NOTES

1. A. Einstein, B. Podolsky, N. Rosen, Can quantum-mechanical description of physical reality be considered complete? *Phys. Rev.* **47**, 777–780 (1935).
2. L. Hardy, Nonlocality for two particles without inequalities for almost all entangled states. *Phys. Rev. Lett.* **71**, 1665–1668 (1993).
3. A. J. Leggett, Nonlocal hidden-variable theories and quantum mechanics: An incompatibility theorem. *Found. Phys.* **33**, 1469–1493 (2003).
4. A. K. Ekert, Quantum cryptography based on Bell's theorem. *Phys. Rev. Lett.* **67**, 661–663 (1991).
5. T. Jennewein, C. Simon, G. Weihs, H. Weinfurter, A. Zeilinger, Quantum cryptography with entangled photons. *Phys. Rev. Lett.* **84**, 4729–4732 (2000).
6. C. H. Bennett, G. Brassard, C. Crèpeau, R. Jozsa, A. Peres, W. K. Wootters, Teleporting an unknown quantum state via dual classical and einstein-podolsky-rosen channels. *Phys. Rev. Lett.* **70**, 1895–1899 (1993).
7. D. Bouwmeester, J.-W. Pan, K. Mattle, M. Eibl, H. Weinfurter, A. Zeilinger, Experimental quantum teleportation. *Nature* **390**, 575–579 (1997).
8. M. Riebe, H. Häffner, C. F. Roos, W. Hänsel, J. Benhelm, G. P. T. Lancaster, T. W. Körber, C. Becher, F. Schmidt-Kaler, D. F. V. James, R. Blatt, Deterministic quantum teleportation with atoms. *Nature* **429**, 734–737 (2004).
9. M. D. Barrett, J. Chiaverini, T. Schaetz, J. Britton, W. M. Itano, J. D. Jost, E. Knill, C. Langer, D. Leibfried, R. Ozeri, D. J. Wineland, Deterministic quantum teleportation of atomic qubits. *Nature* **429**, 737–739 (2004).
10. R. Ursin, T. Jennewein, M. Aspelmeyer, R. Kaltenbaek, M. Lindenthal, P. Walther, A. Zeilinger, Quantum teleportation across the Danube. *Nature* **430**, 849 (2004).
11. C. H. Bennett, S. J. Wiesner, Communication via one- and two-particle operators on Einstein-Podolsky-Rosen states. *Phys. Rev. Lett.* **69**, 2881–2884 (1992).
12. Z. Shadman, H. Kampermann, C. Macchiavello, D. Bruß, Optimal super dense coding over noisy quantum channels. *New J. Phys.* **12**, 073042 (2010).
13. T. B. Pittman, Y. H. Shih, D. V. Strekalov, A. V. Sergienko, Optical imaging by means of two-photon quantum entanglement. *Phys. Rev. A* **52**, R3429–R3432 (1995).
14. J. H. Shapiro, Computational ghost imaging. *Phys. Rev. A* **78**, 061802 (2008).
15. D. Deutsch, A. Ekert, Quantum computation. *Phys. World* **11**, 47–52 (1998).
16. P. Walther, K. J. Resch, T. Rudolph, E. Schenck, H. Weinfurter, V. Vedral, M. Aspelmeyer, A. Zeilinger, Experimental one-way quantum computing. *Nature* **434**, 169–176 (2005).
17. R. Prevedel, P. Walther, F. Tiefenbacher, P. Böhi, R. Kaltenbaek, T. Jennewein, A. Zeilinger, High-speed linear optics quantum computing using active feed-forward. *Nature* **445**, 65–69 (2007).
18. J. Yin, Y. Cao, Y.-H. Li, S.-K. Liao, L. Zhang, J.-G. Ren, W.-Q. Cai, W.-Y. Liu, B. Li, H. Dai, G.-B. Li, Q.-M. Lu, Y.-H. Gong, Y. Xu, S.-L. Li, F.-Z. Li, Y.-Y. Yin, Z.-Q. Jiang, M. Li, J.-J. Jia, G. Ren, D. He, Y.-L. Zhou, X.-X. Zhang, N. Wang, X. Chang, Z.-C. Zhu, N.-L. Liu, Y.-A. Chen, C.-Y. Lu, R. Shu, C.-Z. Peng, J.-Y. Wang, J.-W. Pan, Satellite-based entanglement distribution over 1200 kilometers. *Science* **356**, 1140–1144 (2017).
19. H. Hübel, M. R. Vanner, T. Lederer, B. Blauensteiner, T. Lorünser, A. Poppe, A. Zeilinger, High-fidelity transmission of polarization encoded qubits from an entangled source over 100 km of fiber. *Opt. Express* **15**, 7853–7862 (2007).
20. S. Wengerowsky, S. K. Joshi, F. Steinlechner, J. R. Zichi, B. Liu, T. Scheidl, S. M. Dobrovolskiy, R. van der Molen, J. W. Los, V. Zwiller, M. A. M. Versteegh, A. Mura, D. Calonico, M. Inguscio, A. Zeilinger, A. Xuereb, R. Ursin, Passively stable distribution of polarisation entanglement over 192 km of deployed optical fibre. arXiv:1907.04864 (2019).
21. N. J. Cerf, M. Bourennane, A. Karlsson, N. Gisin, Security of quantum key distribution using *d*-level systems. *Phys. Rev. Lett.* **88**, 127902 (2002).
22. H. Bechmann-Pasquinucci, W. Tittel, Quantum cryptography using larger alphabets. *Phys. Rev. A* **61**, 062308 (2000).
23. V. Parigi, V. D'Ambrosio, C. Arnold, L. Marrucci, F. Sciarrino, J. Laurat, Storage and retrieval of vector beams of light in a multiple-degree-of-freedom quantum memory. *Nat. Commun.* **6**, 7706 (2015).
24. D.-S. Ding, W. Zhang, S. Shi, Z.-Y. Zhou, Y. Li, B.-S. Shi, G.-C. Guo, High-dimensional entanglement between distant atomic-ensemble memories. *Light: Sci. Appl.* **5**, e16157 (2016).
25. J. D. Franson, Bell inequality for position and time. *Phys. Rev. Lett.* **62**, 2205–2208 (1989).
26. R. T. Thew, A. Acin, H. Zbinden, N. Gisin, Bell-type test of energy-time entangled qutrits. *Phys. Rev. Lett.* **93**, 010503 (2004).
27. T. Zhong, H. Zhou, R. D. Horansky, C. Lee, V. B. Verma, A. E. Lita, A. Restelli, J. C. Bienfang, R. P. Mirin, T. Gerrits, S. W. Nam, F. Marsili, M. D. Shaw, Z. Zhang, L. Wang, D. Englund, G. W. Wornell, J. H. Shapiro, F. N. C. Wong, Photon-efficient quantum key distribution using time–energy entanglement with high-dimensional encoding. *New J. Phys.* **17**, 022002 (2015).
28. D. Stucki, H. Zbinden, N. Gisin, A Fabry–Perot-like two-photon interferometer for highdimensional time-bin entanglement. *J. Mod. Opt.* **52**, 2637–2648 (2005).
29. T. Ikuta, H. Takesue, Four-dimensional entanglement distribution over 100 km. *Sci. Rep.* **8**, 817 (2018).
30. C. Lee, D. Bunandar, M. Pavlovich, M. Grein, R. Murphy, S. Hamilton, D. Englund, P. B. Dixon, in *2018 Conference on Lasers and Electro-Optics (CLEO)* (IEEE, 2018), pp. 1–2.
31. P. Imany, J. A. Jaramillo-Villegas, J. M. Lukens, M. S. Alshaykh, O. D. Odele, D. E. Leaird, M. Qi, A. M. Weiner, Deterministic optical quantum logic with multiple high-dimensional degrees of freedom in a single photon. arXiv:1805.04410 (2018).
32. S. Ramelow, L. Ratschbacher, A. Fedrizzi, N. K. Langford, A. Zeilinger, Discrete tunable color entanglement. *Phys. Rev. Lett.* **103**, 253601 (2009).
33. A. Mair, A. Vaziri, G. Weihs, A. Zeilinger, Entanglement of the orbital angular momentum states of photons. *Nature* **412**, 313–316 (2001).
34. G. Molina-Terriza, J. P. Torres, L. Torner, Twisted photons. *Nat. Phys.* **3**, 305–310 (2007).
35. M. Krenn, M. Malik, M. Erhard, A. Zeilinger, Orbital angular momentum of photons and the entanglement of Laguerre–Gaussian modes. *Philos. Trans. A Math. Phys. Eng. Sci.* **375**, 20150442 (2017).
36. M. Erhard, R. Fickler, M. Krenn, A. Zeilinger, Twisted photons: New quantum perspectives in high dimensions. *Light: Sci. Appl.* **7**, 17146 (2018).
37. W. Löffler, T. G. Euser, E. R. Eliel, M. Scharrer, P. S. J. Russell, J. P. Woerdman, Fiber transport of spatially entangled photons. *Phys. Rev. Lett.* **106**, 240505 (2011).
38. Y. Kang, J. Ko, S. M. Lee, S.-K. Choi, B. Y. Kim, H. S. Park, Measurement of the entanglement between photonic spatial modes in optical fibers. *Phys. Rev. Lett.* **109**, 020502 (2012).
39. D. Cozzolino, D. Bacco, B. Da Lio, K. Ingerslev, Y. Ding, K. Dalgaard, P. Kristensen, M. Galili, K. Rottwitt, S. Ramachandran, L. Katsuo, Orbital angular momentum states enabling fiber-based high-dimensional quantum communication. *Phys. Rev. Appl.* **11**, 064058 (2019).
40. M. P. J. Lavery, M. M. Abadi, R. Bauer, G. Brambilla, L. Cheng, M. A. Cox, A. Dudley, A. D. Ellis, N. K. Fontaine, A. E. Kelly, C. Marquardt, S. Matlhane, B. Ndagano, F. Petruccione, R. Slavk, F. Romanato, C. Rosales-Guzmn, F. S. Roux, K. Roux, J. Wang, A. Forbes, Tackling Africas digital divide. *Nat. Photonics* **12**, 249–252 (2018).
41. M. Caleffi, A. S. Cacciapuoti, G. Bianchi, Quantum internet: From communication to distributed computing! arXiv:1805.04360 (2018).
42. A. S. Cacciapuoti, M. Caleffi, F. Tafuri, F. S. Cataliotti, S. Gherardini, G. Bianchi, Quantum internet: Networking challenges in distributed quantum computing. arXiv:1810.08421 (2018).
43. L. Allen, M. W. Beijersbergen, R. J. C. Spreeuw, J. P. Woerdman, Orbital angular momentum of light and the transformation of Laguerre-Gaussian laser modes. *Phys. Rev. A* **45**, 8185–8189 (1992).
44. L. Marrucci, C. Manzo, D. Paparo, Optical spin-to-orbital angular momentum conversion in inhomogeneous anisotropic media. *Phys. Rev. Lett.* **96**, 163905 (2006).
45. S. P. Walborn, M. O. T. Cunha, S. Pdua, C. H. Monken, A double-slit quantum eraser. *Phys. Rev. A* **65**, 033818 (2002).
46. I. Nape, B. Ndagano, A. Forbes, Erasing the orbital angular momentum information of a photon. *Phys. Rev. A* **95**, 053859 (2017).

47. R. C. Devlin, A. Ambrosio, N. A. Rubin, J. P. B. Mueller, F. Capasso, Arbitrary spin-to-orbital angular momentum conversion of light. *Science* **358**, 896–901 (2017).
48. G. Ruffato, M. Girardi, M. Massari, E. Mafakheri, B. Sephton, P. Capaldo, A. Forbes, F. Romanato, A compact diffractive sorter for high-resolution demultiplexing of orbital angular momentum beams. *Sci. Rep.* **8**, 10248 (2018).
49. J. Calsamiglia, Generalized measurements by linear elements. *Phys. Rev. A* **65**, 030301 (2002).
50. D. Giovannini, J. Romero, J. Leach, A. Dudley, A. Forbes, M. J. Padgett, Characterization of highdimensional entangled systems via mutually unbiased measurements. *Phys. Rev. Lett.* **110**, 143601 (2013).
51. Y. Zhang, M. Agnew, T. Roger, F. S. Roux, T. Konrad, D. Faccio, J. Leach, A. Forbes, Simultaneous entanglement swapping of multiple orbital angular momentum states of light. *Nat. Commun.* **8**, 632 (2017).
52. R. Jozsa, Fidelity for mixed quantum states. *J. Mod. Opt.* **41**, 2315–2323 (1994).
53. D. F. James, P. G. Kwiat, W. J. Munro, A. G. White, in *Asymptotic Theory of Quantum Statistical Inference: Selected Papers* (World Scientific, 2005), pp. 509–538.
54. B. Jack, J. Leach, H. Ritsch, S. Barnett, M. Padgett, S. Franke-Arnold, Precise quantum tomography of photon pairs with entangled orbital angular momentum. *New J. Phys.* **11**, 103024 (2009).
55. J. F. Clauser, M. A. Horne, A. Shimony, R. A. Holt, Proposed experiment to test local hidden-variable theories. *Phys. Rev. Lett.* **23**, 880–884 (1969).
56. J. Leach, B. Jack, J. Romero, M. Ritsch-Marte, R. W. Boyd, A. Jha, S. Barnett, S. Franke-Arnold, M. Padgett, Violation of a bell inequality in two-dimensional orbital angular momentum state-spaces. *Opt. Express* **17**, 8287–8293 (2009).

Acknowledgments

Funding: This work was supported by the Key R&D Program of Guangdong Province (2018B030325002), the National Natural Science Foundation of China (NSFC) (61761130082, 11574001, and 11774116), the Royal Society-Newton Advanced Fellowship, the National Program for Support of Top-notch Young Professionals, the Natural Science Foundation of Hubei Province of China (2018CFA048), the Program for HUST Academic Frontier Youth Team (2016QYTD05), the Fundamental Research Funds for the Central Universities (2019kfyRCPY037), the Claude Leon Foundation, and the Department of Science and Technology (South Africa). **Author contributions:** J.L., I.N., Q.W., and A.V. performed the experiments and contributed to data analysis and writing of the paper. J.W. and A.F. developed the concept, conceived the experiment, finalized the paper, and supervised the project. **Competing interests:** The authors declare that they have no competing interests. **Data and materials availability:** All data needed to evaluate the conclusions in the paper are present in the paper and/or the Supplementary Materials. Additional data related to this paper may be requested from J.W.

Submitted 18 May 2019
Accepted 1 November 2019
Published 24 January 2020
10.1126/sciadv.aay0837

Citation: J. Liu, I. Nape, Q. Wang, A. Vallés, J. Wang, A. Forbes, Multidimensional entanglement transport through single-mode fiber. *Sci. Adv.* **6**, eaay0837 (2020).